

Interaction of toroidal swimmers in Stokes flow

Jianjun Huang*

Department of Mathematical Sciences, Worcester Polytechnic Institute, Worcester, Massachusetts 01609, USA

Lisa Fauci†

Department of Mathematics, Tulane University, New Orleans, Louisiana 70118, USA

(Received 4 November 2016; published 5 April 2017)

A doughnut-shaped object supporting surface rotations was a hypothetical construct proposed by both Taylor and Purcell as a swimmer that would be able to propel itself in a Stokesian fluid because of the irreversibility of its stroke. Here we numerically examine the hydrodynamic interaction of pairs and trios of these free toroidal swimmers. First, we study the axisymmetric case of two toroidal swimmers placed in tandem, and show that a single torus of a corotating pair is more efficient than when it swims alone, but less efficient when paired with a counterrotating partner. Using a regularized Stokeslet framework, we study the nonaxisymmetric case of toroidal swimmers whose axes are initially parallel, but not collinear. These perturbed in tandem swimmers can exhibit qualitatively different trajectories that may, for instance, repel the swimmers or have them settle into a periodic state. We also illustrate interesting dynamics that occur for different initial configurations of three tori.

DOI: [10.1103/PhysRevE.95.043102](https://doi.org/10.1103/PhysRevE.95.043102)**I. INTRODUCTION**

Interest in the fluid dynamics of motile microorganisms has surged in recent years [1]. Microfluidic devices have enabled researchers to precisely control physical and chemical environments that can probe microbial processes at the microscale [2,3]. Harnessing the motility of bacteria or eukaryotic microorganisms to transport microscale loads presents an intriguing possibility for drug delivery [4,5]. In addition to using nature's own swimmers for targeted delivery, fabricated helical micromachines that can move colloidal microparticles by magnetic actuation have been engineered [6]. The understanding of the mechanics and energetics of microswimmers, both natural or fabricated, is essential for the exploitation and manipulation of their motility in biotechnology.

At the length scale of microorganisms, inertia is negligible and viscous forces dominate. In this Stokes regime, swimming progress can only occur with a stroke that is irreversible in time. In his classic work that initiated the mathematical analysis of the fluid dynamics of microorganisms, Taylor sketched a hypothetical simple swimmer that was a cylinder bent so that its axis forms a circle [7]. If the cross-sectional rings of the torus rotate with a constant angular velocity, would this toroidal animal propel itself in a viscous, incompressible fluid? Purcell also considered the propulsion of such a hypothetical animal, whose surface rotation is a simple example of a stroke that breaks time-reversal symmetry [8]. Analysis has demonstrated that the toroidal swimmer will, indeed, propel itself in the direction opposite to the rotational direction of its outer surface [9–11].

The construct of the toroidal swimmer, although idealized, can shed light on some true biological systems. For instance, a dinoflagellate swims due to the action of two flagella, a transverse flagellum and a longitudinal flagellum [12–18]. The longitudinal flagellum trails behind the cell body and prop-

agates planar waves, much like a sperm flagellum. Wrapped around the equator of the spherical cell body in a plane perpendicular to the longitudinal flagellum, the transverse flagellum propagates helical waves. The microbe is observed to swim forward in the direction opposite the longitudinal flagellum, and also to rotate about its longitudinal axis. The forward progression had previously been attributed to the longitudinal flagellum, with rotation being attributed to the transverse flagellum [16]. However, recent analysis and computations have shown that the transverse flagellum contributes to the forward motion [17,18]. A torus propagating surface rotation captures many features of the waving transverse flagellum of the dinoflagellate [18]. In another context, the construction of a toroidal swimmer out of DNA miniplasmids has been proposed as a nanomachine whose surface rotations can be driven by periodic temperature changes [19].

When a microswimmer is not isolated, but moving as part of a collection, swimming trajectories and energetics are altered due to hydrodynamic interactions [20–23]. Here we study the fluid dynamics of the interaction of toroidal swimmers in Stokes flow [24]. Using a regularized Stokeslet framework [25], we examine the motility of pairs of toroidal free swimmers whose axes are initially parallel, but not necessarily collinear. We show that perturbed in-tandem swimmers can follow qualitatively different trajectories that, for instance, repel the swimmers or have them periodically move towards and away from each other. In addition, we show that three tori swimming in tandem can exhibit intriguing dynamics due to their interaction. We offer these toroidal swimmers as the three-dimensional (3D) Stokes counterparts of the 2D finite-dipole inviscid swimmers presented by Tchieu *et al.* [26].

II. MATHEMATICAL MODEL

Figure 1 shows a torus formed by the rotation of a small circle of radius r_h about an axis. The circular trajectory of its center is referred to as the centerline of the torus, and its radius is denoted by r_c . On the surface of each torus a fixed

*jhuang3@tulane.edu

†fauci@tulane.edu

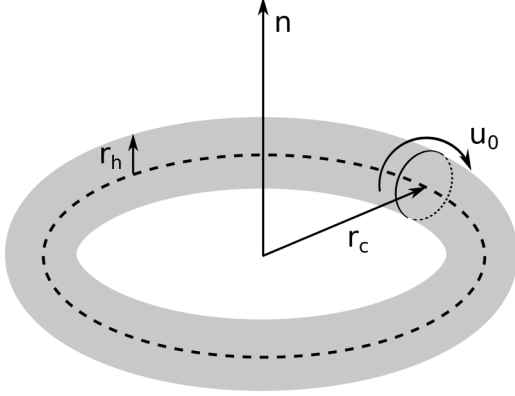


FIG. 1. A schematic diagram of the rotating torus with radius of the tube r_h , radius of the centerline r_c , normal direction \mathbf{n} , and surface tangential velocity \mathbf{u}_0 . The dashed line is the centerline of the torus.

rotational velocity \mathbf{u}_0 about the centerline will be imposed. The normal vector of the torus \mathbf{n} points in the direction of the axis perpendicular to the plane of the circular centerline. We choose the normal vector direction to coincide with the direction of the imposed velocity at the inner surface of the torus.

The surface of the torus ∂D supports forces \mathbf{F} that are exerted on the viscous fluid in which it is immersed. These forces are not preset, but will be determined so that the prescribed surface velocity is achieved along with conservation of momentum and angular momentum. Because the length and velocity scales at the microscopic level are so small, the flow is governed by the incompressible Stokes equations:

$$-\nabla p + \mu \Delta \mathbf{u} + \mathbf{f}(\mathbf{x}, t) = 0 \quad (1)$$

$$\nabla \cdot \mathbf{u} = 0.$$

Here \mathbf{u} is the fluid velocity, p is pressure, μ is the dynamic viscosity and \mathbf{f} is a force density that represents the force of the toroidal swimmer on the fluid.

This force density is supported on the surface of the torus and is given by:

$$\mathbf{f}(\mathbf{x}, t) = \int_{\partial D} \mathbf{F}(\mathbf{X}(\mathbf{s}, t), t) \psi_\epsilon(\mathbf{x} - \mathbf{X}(\mathbf{s}, t)) ds. \quad (2)$$

Material points on the surface of the torus ∂D are denoted by $\mathbf{X}(\mathbf{s}, t)$, where \mathbf{s} is a two-dimensional Lagrangian surface parameter. Here ψ_ϵ is a regularized three-dimensional Dirac δ function that distributes the force in a small volume around a material point of the toroidal surface [25]. We choose:

$$\psi_\epsilon(\mathbf{x}) = \frac{15\epsilon^4}{8\pi(r^2 + \epsilon^2)^{7/2}}, \quad (3)$$

where $r = \|\mathbf{x}\|$. For this choice of regularization, the velocity $\mathbf{u} = (u_1, u_2, u_3)$ due to a single regularized force $\mathbf{f} = \mathbf{f}_0 \psi_\epsilon(\mathbf{x} - \mathbf{x}_0)$ applied at the point \mathbf{x}_0 is:

$$u_i(\mathbf{x}) = \frac{1}{8\pi\mu} S_{ij}^\epsilon(\mathbf{x}, \mathbf{x}_0) f_{0j},$$

where the regularized Stokeslet is given by:

$$S_{ij}^\epsilon(\mathbf{x}, \mathbf{x}_0) = \delta_{ij} \frac{r^2 + 2\epsilon^2}{(r^2 + \epsilon^2)^{3/2}} + \frac{(\mathbf{x}_i - \mathbf{x}_{0,i})(\mathbf{x}_j - \mathbf{x}_{0,j})}{(r^2 + \epsilon^2)^{3/2}}. \quad (4)$$

Here δ_{ij} is the Kronecker delta, $r = \|\mathbf{x} - \mathbf{x}_0\|$ and $\tilde{x}_i = x_i - x_{0,i}$. The velocity is defined at all points $\mathbf{x} \in \mathbb{R}^3$, even at $\mathbf{x} = \mathbf{x}_0$, due to the regularization. For $\epsilon = 0$ the regularized Stokeslet in Eq. (4) reduces to the classical singular Stokeslet [28].

For a distribution of forces applied on the surface ∂D of the torus:

$$u_i(\mathbf{x}, t) = \frac{1}{8\pi\mu} \int_{\partial D} S_{ij}^\epsilon(\mathbf{x}, \mathbf{X}(\mathbf{s}, t)) F_j(\mathbf{X}(\mathbf{s}, t), t) ds. \quad (5)$$

In practice, the surface of the torus is discretized by N material points and the evaluation of Eq. (5) at these material points results in a linear system relating the imposed velocities at these surface points to the forces at those points:

$$\mathbb{L} \mathbf{F} = \mathbf{v}. \quad (6)$$

Here \mathbb{L} is a $3N \times 3N$ matrix,

$$\mathbf{F} = (F_1^1, F_2^1, F_3^1, \dots, F_1^N, F_2^N, F_3^N)^T$$

and

$$\mathbf{v} = (u_1^1, u_2^1, u_3^1, \dots, u_1^N, u_2^N, u_3^N)^T,$$

where F_j^i and u_j^i are the j th ($j = 1, 2, 3$) component of the surface force and velocity, respectively, of the i th ($i = 1, 2, \dots, N$) point. The matrix \mathbb{L} depends only upon the positions of the discrete points of the toroidal surface. Because we are modeling a free toroidal swimmer, we require that the total force and torque be zero. In order to satisfy these constraints, the toroidal swimmer undergoes a rigid translation and rotation. We denote the overall velocity of a toroidal surface point as $\mathbf{u} = \mathbf{u}_0 + \mathbf{U} + \Omega \times (\mathbf{x} - \mathbf{x}_c)$, where \mathbf{u}_0 is the imposed tangential velocity, \mathbf{U} is the induced translational velocity, Ω is the induced rotational velocity and \mathbf{x}_c is the center of the object. The rigid translation and rotation add six unknowns to the system so that the six constraints due to force-free and torque-free swimming can be met.

The equations (6) together with the six equations ensuring conservation of linear and angular momentum can be presented as:

$$A \tilde{\mathbf{F}} = \tilde{\mathbf{v}}. \quad (7)$$

Here, A is a $(3N + 6) \times (3N + 6)$ symmetric matrix, and

$$\tilde{\mathbf{F}} = (F_1^1, F_2^1, F_3^1, \dots, F_1^N, F_2^N, F_3^N, \mathbf{U}, \Omega)^T$$

$$\tilde{\mathbf{v}} = (u_1^1, u_2^1, u_3^1, \dots, u_1^N, u_2^N, u_3^N, 0, 0, 0, 0, 0, 0)^T.$$

This system of equations allows us to compute the forces that must be exerted at the material points of the toroidal surface to achieve the imposed surface velocity \mathbf{u}_0 , along with the resulting translation and rotation of the swimmer. Moreover, the computed force distribution $\tilde{\mathbf{F}}$ allows us to evaluate the fluid velocity at any point in \mathbb{R}^3 using a discretized version of Eq. (5).

III. SINGLE TORUS

We nondimensionalize the Stokes equations (1) by choosing a length scale L , a velocity scale U , a time scale $T = L/U$, a pressure scale $P = \mu U/L$, and a force scale $F = \mu U/L^2$. In

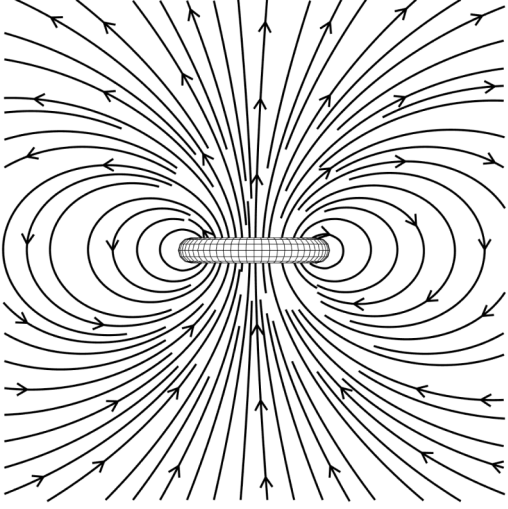


FIG. 2. Streamlines and flow directions in the plane $y = 0$ around a force-free torus with aspect ratio $s_0 = 5$. The solid lines are the streamlines of the flow around the toroidal swimmer. The arrows indicate the direction of the flow.

this nondimensional setting, we consider a single torus of unit diameter (i.e., radius $r_c = 0.5$) and tube radius $r_h = 0.1$, so that its aspect ratio $s_0 = r_c/r_h = 5$. A uniform surface tangential speed of $u_0 = 100$ is imposed. The center and the normal of the torus are assumed to be $\mathbf{x}_c = (0,0,0)$ and $\mathbf{n} = (0,0,1)$, respectively. Figure 2 shows instantaneous streamlines and flow directions around this free-swimming torus calculated using the method of regularized Stokeslets where the surface of the torus was discretized with $M_h = 12$ points on each cross-sectional circle and $M_c = 60$ cross-sectional circles around the centerline, for a total of $N = 720$ nodes. Neighboring nodes both around the circular cross sections and between cross sections were nearly equally spaced with grid distance $\Delta s \approx 0.05$. As in previous regularized Stokeslet models that relate surface velocities to surface forces [18,25,29,30], the regularization parameter ϵ was chosen to be a multiple of Δs . Here we chose $\epsilon \approx 0.35\Delta s$.

By considering a distribution of rotlets along the torus centerline, Kulic *et al.* [19] showed that in the limit of large aspect ratio s_0 , the free-swimming torus powered by surface rotation of speed u_0 would translate at the velocity:

$$U = \frac{u_0}{2s_0} \left(\log(8s_0) - \frac{1}{2} \right) \quad (8)$$

in the direction of its inner surface motion. Later, Leshansky and Kenneth [11] used toroidal coordinates to calculate the free-swimming speed of the toroidal swimmer without the same large aspect ratio assumption. Given the parameters of the torus described above, the asymptotic translational velocity from Eq. (8) is $U = 31.89$. Even for this moderate value of aspect ratio $s_0 = 5$, the regularized Stokeslet calculation shows excellent agreement with a computed value of $U = 31.34$. Note that symmetry restricts the translational velocity of the torus to be only in the z direction, as well as the angular velocity $\Omega = 0$.

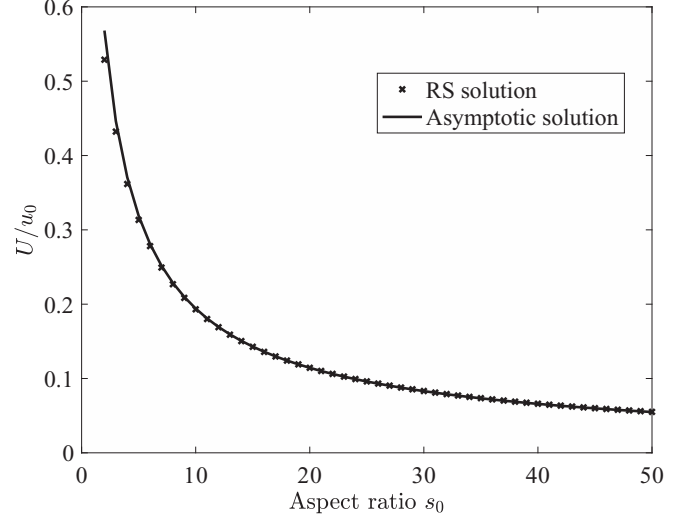


FIG. 3. Ratio of propulsive velocity to surface velocity (U/u_0) versus aspect ratio $s_0 = \frac{r_c}{r_h}$. The solid curve uses the asymptotic solution in Eq. (8) and the crosses indicate regularized Stokeslet (RS) computations.

Figure 3 shows the ratio of propulsive velocity to surface velocity U/u_0 computed for a series of aspect ratios using the method of regularized Stokeslets. The tube radius of the tori was held fixed, but the radius of the centerline increased to achieve the larger aspect ratios. More cross-sectional circles were added as the centerline radius increased, keeping the distance between nodes Δs unchanged. The solid curve in Fig. 3 indicates the asymptotic value of the ratio, whereas the crosses indicate the values computed using the numerical method. Along with convergence studies that varied the surface discretization and blob size, this comparison with theory allowed us to calibrate the numerical parameters so that the calculations are sufficiently resolved [24].

IV. INTERACTION OF MULTIPLE TORI

The coupled torus-Stokes system for a single torus presented above is easily extended to study the interaction of multiple free-swimming tori in a Stokesian fluid by summing over the contribution of each torus surface to the force density in the Stokes equations (1):

$$\mathbf{f}(\mathbf{x}, t) = \sum_{k=1}^{N_t} \int_{\partial D_k} \mathbf{F}_k(\mathbf{X}_k(\mathbf{s}, t), t) \psi_\epsilon(\mathbf{x} - \mathbf{X}_k(\mathbf{s}, t)) ds. \quad (9)$$

Here N_t is the number of tori, and the material points on the surface of the k th torus ∂D_k are denoted by $\mathbf{X}_k(\mathbf{s}, t)$. The total force and torque on each of the N_t tori, separately, is zero. The resulting translational and rotational velocities, \mathbf{U}_k and Ω_k , are computed for $k = 1, 2, \dots, N_t$.

A. Two tori placed in tandem

We first examine two identical tori rotating with the same surface velocity, placed in tandem so that their normal vectors are collinear. We assume the normal vectors $\mathbf{n}_1 = \mathbf{n}_2 = (0,0,1)$ are aligned with the z axis. A pair of corotating tori are shown

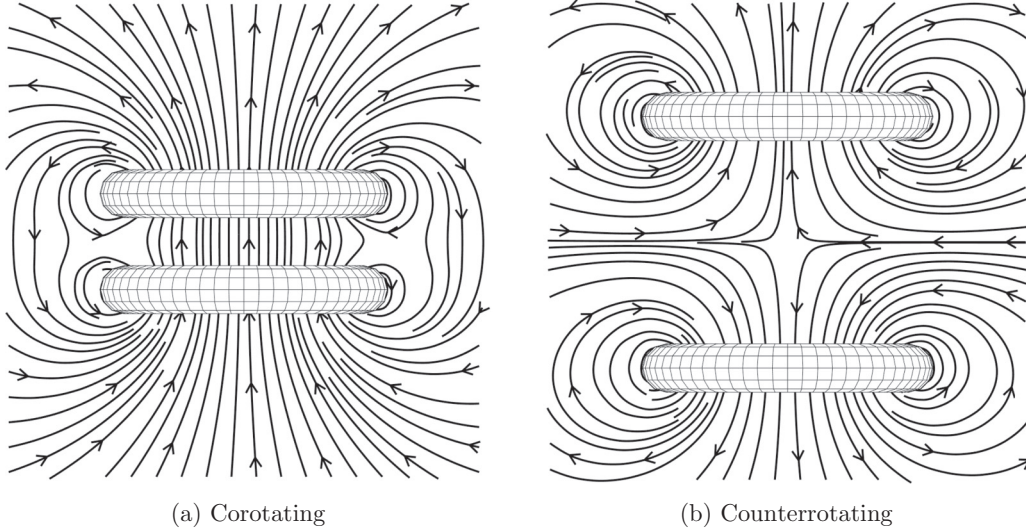


FIG. 4. (a) Streamlines around two corotating tori. This pair translates upwards at a constant speed with no rotation, and the distance between their centers remains fixed. (b) Streamlines around two counterrotating tori. Each torus in this pair will be moving away from the other at the same speed, and this speed will depend upon the distance between their centers. Arrows indicate the direction of flow.

in Fig. 4(a). Symmetry considerations and the reversibility of Stokes flow dictate that the translational velocities $\mathbf{U}_1 = \mathbf{U}_2 = (0,0,U)$ and that the rotational velocities $\boldsymbol{\Omega}_1 = \boldsymbol{\Omega}_2 = \mathbf{0}$. In this case, the two tori translate upwards as a pair, maintaining a constant distance between their centers. Their velocities remain unchanged as they translate. Similarly, we examine two identical tori rotating with opposite surface velocities, also placed in tandem but with $\mathbf{n}_1 = -\mathbf{n}_2$. A pair of counterrotating tori along with the extensional flow they create are shown in Fig. 4(b). In this case, symmetry considerations and Stokes reversibility give $\mathbf{U}_1 = (0,0,U) = -\mathbf{U}_2$ and $\boldsymbol{\Omega}_1 = \boldsymbol{\Omega}_2 = \mathbf{0}$. Depending upon the direction of the surface rotations, the counterrotating tori either move towards each other or away from each other [as in Fig. 4(b)].

The velocities of both the corotating or counterrotating pair of free-swimming, in-tandem, tori were computed by Thaokar [31] using asymptotics for slender tori in the far-field limit, as well as using boundary integral methods for nonslender tori with separation distance on the order of the toroidal radius. In these calculations, the axisymmetry of the in-tandem arrangement of the toroidal pairs was exploited [31]. It was shown that corotating tori enjoy a boost in speed compared to the speed of a single swimmer. In addition, it was shown that as counterrotating tori move towards each other, their velocity decreases.

We consider in-tandem pairs of both corotating and counterrotating tori of unit diameter (i.e., radius $r_c = 0.5$), aspect ratio $s_0 = 5$ and surface tangential speed $u_0 = 100$, and vary their vertical distance. Figure 5 shows the swimming speeds of both the corotating pair and the counterrotating pair normalized by the speed of an identical isolated torus. Note that the velocities of each torus in the corotating pair are identical, but the velocities of each torus in the counterrotating pair are negative of each other. We see that the corotating pair placed at a distance of $d = 1$ apart realizes a six percent increase in swimming speed when compared to the isolated torus. In addition, we see that counterrotating tori impede each other's

speed when they are close together. When the vertical distance between the tori is more than about six toroidal diameters apart, their speed is nearly that of an isolated torus. We also compare our computations of the speeds of both pairs with the far-field limit reported by Thaokar [31]:

$$U = \frac{u_o}{2s_0} \left(\log 8s_0 - \frac{1}{2} \right) \pm \frac{\pi u_o}{s_0} \left(\frac{11 + 2\tilde{d}^2}{2(4 + \tilde{d}^2)^{5/2}} \right). \quad (10)$$

The agreement was within three percent (see Fig. 5). Here, \tilde{d} is the normalized distance between the centers of two tori by

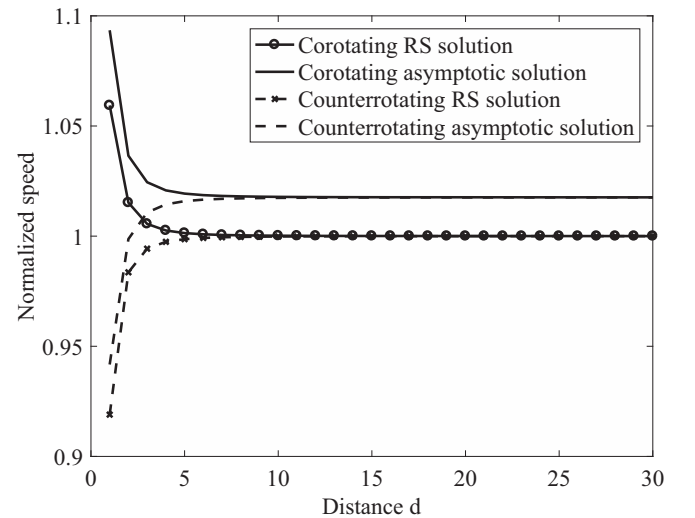


FIG. 5. Swimming speeds of in-tandem corotating (solid line with circles) and counterrotating (dashed line with crosses) torus normalized by the swimming speed of an identical isolated torus as a function of vertical distance. The solid and dashed lines are plotted from formula (10) normalized by the speed of an isolated torus. Here each torus in the pair was of unit diameter and aspect ratio $s_0 = 5$.

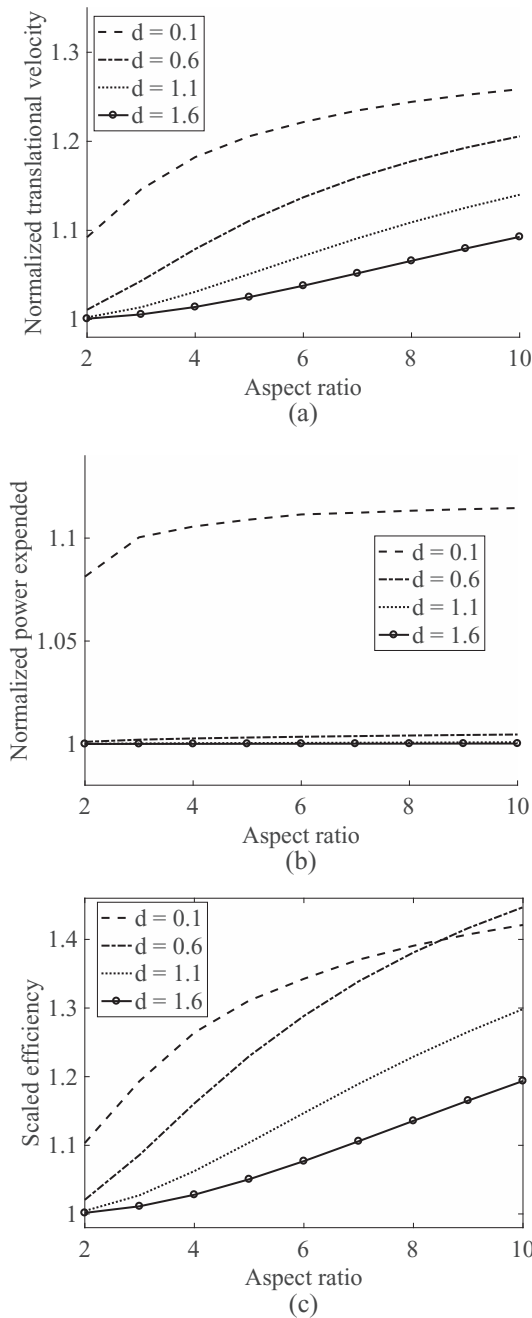


FIG. 6. (a) The swimming speed of an individual torus in an in-tandem corotating pair normalized by the swimming speed of an identical isolated torus as a function of aspect ratio. (b) The power expenditure of an individual torus in an in-tandem corotating pair normalized by the power expenditure of an identical isolated torus as a function of aspect ratio. (c) The efficiency of an individual torus in an in-tandem corotating pair normalized by the efficiency of an identical isolated torus as a function of aspect ratio. The normalized values of speed, power, and efficiency are shown for four different vertical distances between the centers of the tori.

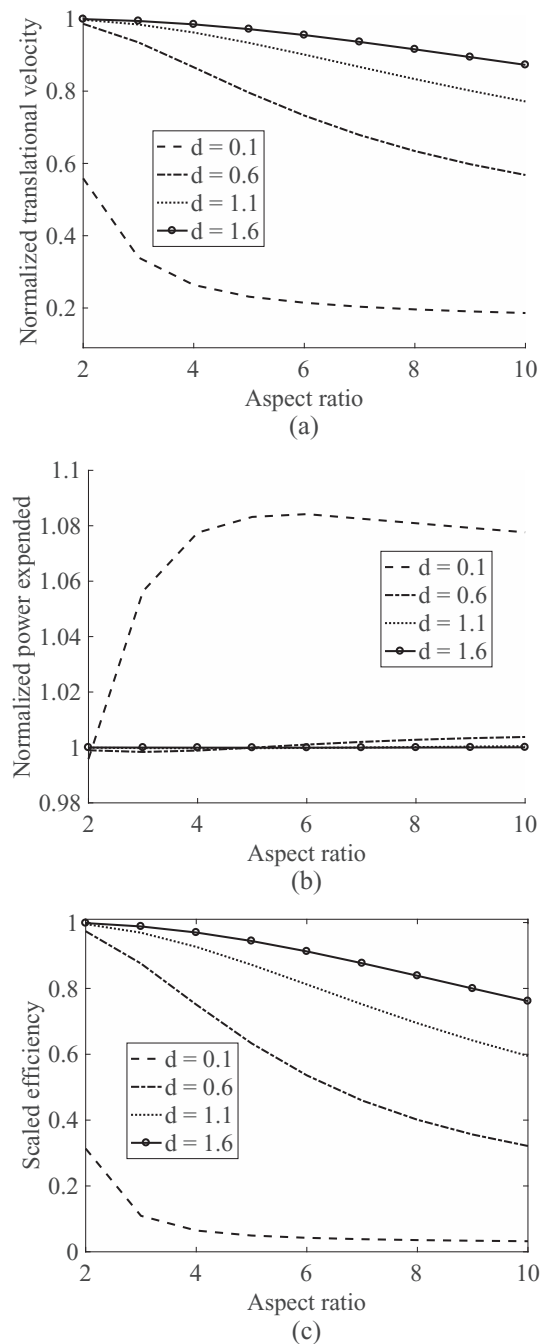


FIG. 7. (a) The swimming speed of an individual torus in an in-tandem counterrotating pair normalized by the swimming speed of an identical isolated torus as a function of aspect ratio. (b) The power expenditure of an individual torus in an in-tandem counterrotating pair normalized by the power expenditure of an identical isolated torus as a function of aspect ratio. (c) The efficiency of an individual torus in an in-tandem counterrotating pair normalized by the efficiency of an identical isolated torus as a function of aspect ratio. The normalized values of speed, power, and efficiency are shown for four different vertical distances between the centers of the tori.

the radius of centerline, i.e., $\tilde{d} = \frac{d+2r_h}{r_c}$, where d is the distance between two tori.

An individual in a pair of corotating tori enhances the swimming speed of its partner. We can also ask how swimming

in tandem changes the power expenditure of each individual in the pair in order to achieve the same surface rotational velocity. Is it more efficient for a torus to swim alone, or find a corotating partner? What about a counterrotating partner? We

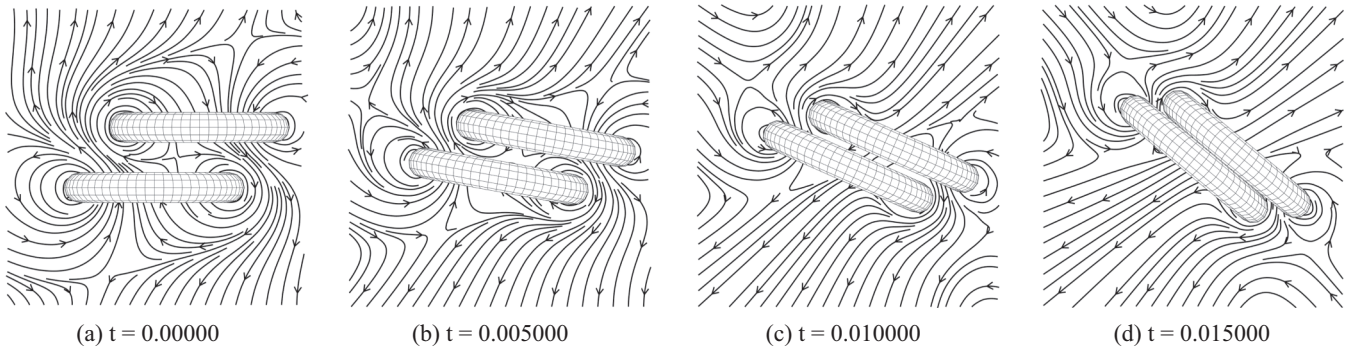


FIG. 8. Two counterrotating tori are initially placed in a perturbed in-tandem configuration so that their normal vectors are parallel but not collinear. The direction of surface rotations causes them to move towards each other. The surrounding streamlines are shown, and the velocity directions are indicated by arrows.

compute the power expended by the k th free-swimming torus undergoing surface rotations as:

$$P_k = \int_{\partial D_k} \mathbf{F}_k \cdot \mathbf{u}_0 ds,$$

where \mathbf{u}_0 is the surface tangential velocity. The swimming efficiency of that torus is then $E_k = U_k^2/P_k$.

Figure 6(a) shows the swimming speed of an individual torus in an in-tandem, corotating pair normalized by the swimming speed of an identical isolated torus. Values of this normalized speed as a function of aspect ratio are denoted for four different vertical distances between the tori. Although the absolute swimming speed of a torus decreases as the aspect ratio increases, we see that the boost in normalized swimming speed increases with aspect ratio, and is more pronounced when the tori are closest together. Figure 6(b) shows the power expenditure of an individual torus in an in-tandem, corotating pair normalized by the power expenditure of an identical isolated torus. We see that the normalized power does not change much with aspect ratio. However, the relative power expenditure for a single torus in the pair is increased by about ten percent for the closest pair ($d = 0.1$). Figure 6(c) shows that, indeed, it is more efficient for a torus to swim as part of an in-tandem, corotating pair rather than alone. This boost in efficiency increases with aspect ratio.

Figure 7(a) shows the swimming speed of an individual torus in an in-tandem, counterrotating pair normalized by the

swimming speed of an identical isolated torus. Values of this normalized speed as a function of aspect ratio are denoted for four different vertical distances between the tori. We see that in all cases the counterrotating tori inhibit each other's speed, especially those placed closest together. This decrease in normalized speed increases with aspect ratio. Note that these values reported are instantaneous for the given vertical distance between tori. This distance would evolve as the pair either approached each other or moved apart, depending upon the directions of surface rotation. Figure 7(b) shows that the relative power expenditure of an individual torus in an in-tandem, counterrotating pair increases with increasing aspect ratio before leveling off for the closest pair of counterrotating tori. Figure 7(c) shows that it is never more efficient for a torus to swim as part of an in-tandem, counterrotating pair rather than alone. For each fixed vertical distance, the relative efficiency decreases with aspect ratio.

B. Two tori: Perturbed in-tandem placement

Two perfectly in-tandem corotating or counterrotating tori, where the normal vectors are collinear, are axisymmetric systems. Here we consider a perturbation of this in-tandem configuration, where the normal vectors of the tori are parallel, but not collinear. Axisymmetry is lost. We assume that the plane determined by the line connecting the tori centers and the parallel normal vectors emanating from their centers is $y = 0$. This two-tori system is then perfectly symmetric about

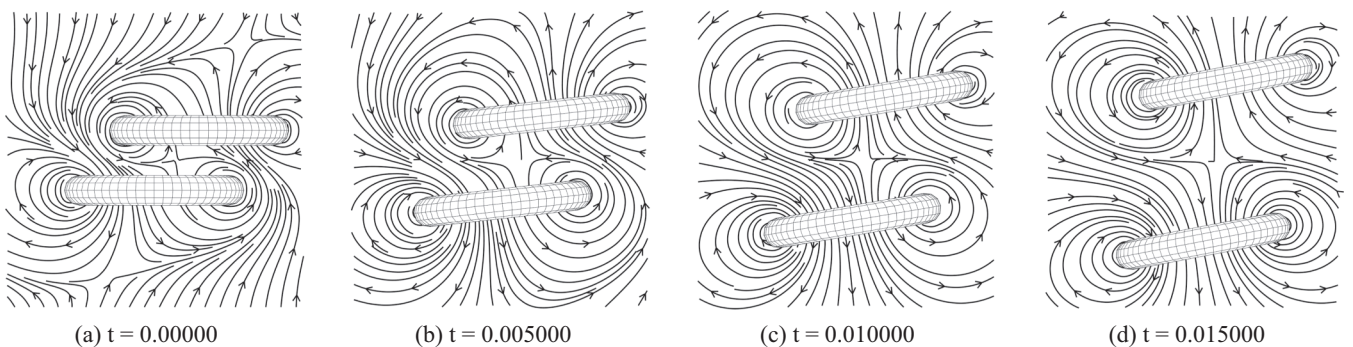


FIG. 9. Two counterrotating tori are initially placed in a perturbed in-tandem configuration so that their normal vectors are parallel but not collinear. The direction of surface rotations are opposite to those in Fig. 8 so that these tori move away from each other. The surrounding streamlines are shown, and the velocity directions are indicated by arrows.

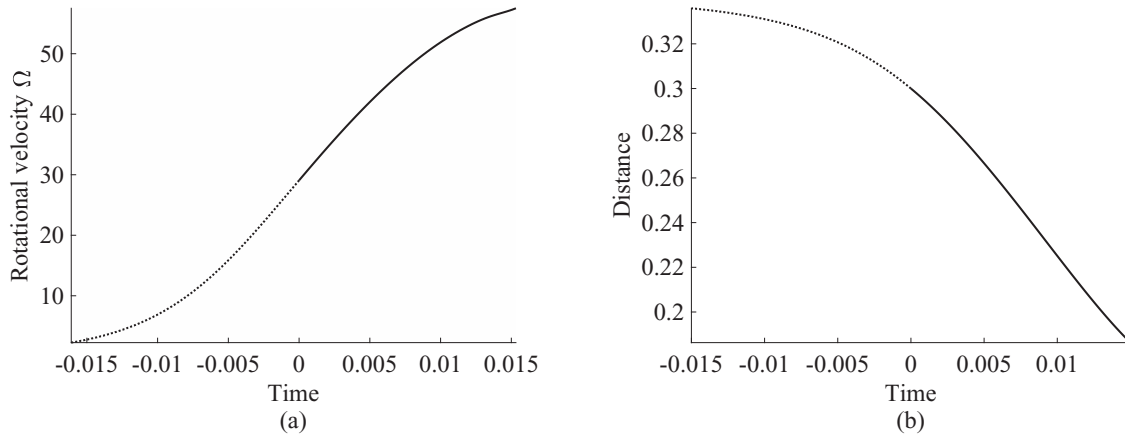


FIG. 10. (a) The rotational velocity of the counterrotating pair of tori in Fig. 8 and Fig. 9. The dashed part of the curve corresponds to running time backwards in Fig. 9. (b) The distance between the parallel normals of the tori.

$y = 0$, and because of this symmetry we can assert that (i) the resulting translational velocity of each tori \mathbf{U}_1 and \mathbf{U}_2 must be zero in the y direction and (ii) the resulting rotation of the pair can only be about the y axis, so the rotational velocity $\boldsymbol{\Omega}_1$ and $\boldsymbol{\Omega}_2$ only have a nonzero in the second component.

Before presenting results of computational simulations that will illustrate the dynamics of such toroidal pairs, we first consider other symmetries of the toroidal placement. A pair of counterrotating tori perturbed from in-tandem placement is shown in Fig. 8(a). Suppose the bottom left torus has instantaneous translational and rotational velocities of $\mathbf{U}_1 = (u_1, 0, v_1)$ and $\boldsymbol{\Omega}_1 = (0, \omega_1, 0)$ and the top right torus has instantaneous translational and rotational velocities of $\mathbf{U}_2 = (u_2, 0, v_2)$ and $\boldsymbol{\Omega}_2 = (0, \omega_2, 0)$. If we rotate the reference frame about the y axis clockwise by π (when viewing the figure), the angular velocities in the new frame $\boldsymbol{\Omega}_1^*$ and $\boldsymbol{\Omega}_2^*$ do not change ($\boldsymbol{\Omega}_1^* = \boldsymbol{\Omega}_1$ and $\boldsymbol{\Omega}_2^* = \boldsymbol{\Omega}_2$), but the translational velocities \mathbf{U}_1^* and \mathbf{U}_2^* switch by a minus sign ($\mathbf{U}_1^* = -\mathbf{U}_1$ and $\mathbf{U}_2^* = -\mathbf{U}_2$). However, this rotated system is now precisely the original system with the positions of the two tori interchanged. We then conclude that $\boldsymbol{\Omega}_1 = \boldsymbol{\Omega}_2$ and $\mathbf{U}_1 = -\mathbf{U}_2$. The tori have the same angular velocity and rotate as a pair, but their velocities are opposing.

Figure 8 shows a sequence of snapshots of such a pair of counterrotating tori of aspect ratio $s_0 = 5$. Because of the direction of surface rotations, each tori in the pair moves closer

to the other at the same speed, and the pair rotates clockwise about the y axis. This speed decreases as they approach each other. Figure 9 shows a sequence of snapshots of the same pair of counterrotating tori, but with surface velocities reversed so that they move away from each other. Because of the reversibility of Stokes flow, we may consider the sequence in Fig. 9 as an extension of the dynamics shown in Fig. 8 with time moving backwards. Using this perspective, we plot the rotational velocity of the pair as a function of time in Fig. 10(a). We see that as the tori approach each other the rotation rate increases. In addition, we do observe a tendency of the tori to align as they approach each other. Figure 10(b) shows the distance between the parallel normals of two tori. As the two tori approach, the flow created by their surface rotations is very nearly an extensional flow. The dynamics of the rotating pair of tori is very much like the dynamics of a pair of microscale rotors that are formed by micron-scale gold and platinum rods that induce an extensional flow due to chemical reactions on their surface [32].

Next we consider the dynamics of a pair of a corotating tori perturbed from in-tandem placement as shown in Fig. 11(a). Suppose the bottom left torus has instantaneous translational and rotational velocities of $\mathbf{U}_1 = (u_1, 0, v_1)$ and $\boldsymbol{\Omega}_1 = (0, \omega_1, 0)$ and the top right torus has instantaneous translational and rotational velocities of $\mathbf{U}_2 = (u_2, 0, v_2)$ and $\boldsymbol{\Omega}_2 = (0, \omega_2, 0)$. As in the counterrotating case, if we rotate the reference frame

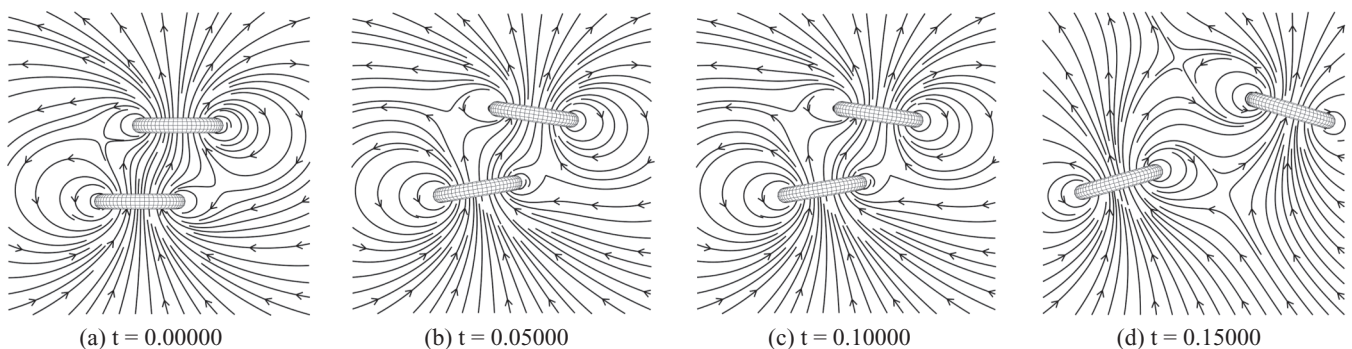


FIG. 11. Two corotating tori of unit diameter are placed so that the offset between their centers in the vertical direction is $h_1 = 1$, and the offset between their centers in the x direction is $h_2 = 0.5$.

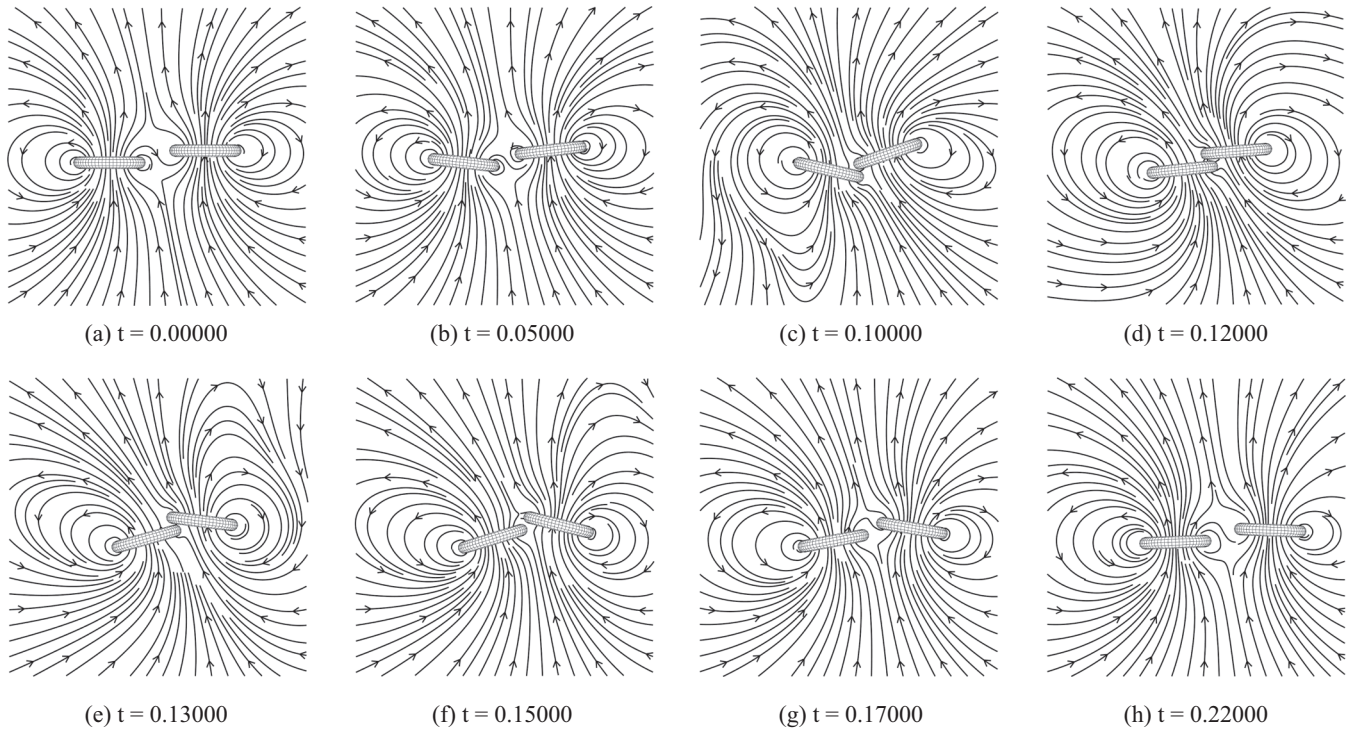


FIG. 12. Two corotating tori of unit diameter are placed so that the offset between their centers in the vertical direction is $h_1 = 0.2$, and the offset between their centers in the x direction is $h_2 = 1.6$. The frame view is moving upwards at a speed of 30. Here the toroidal pair continues on with a periodic trajectory relative to each other as they move upwards.

about the y axis clockwise by π (when viewing the figure), the angular velocities in the new frame Ω_1^* and Ω_2^* do not change ($\Omega_1^* = \Omega_1$ and $\Omega_2^* = \Omega_2$), but the translational velocities \mathbf{U}_1^* and \mathbf{U}_2^* switch by a minus sign ($\mathbf{U}_1^* = -\mathbf{U}_1$ and $\mathbf{U}_2^* = -\mathbf{U}_2$). This rotated system is nearly the original system with the positions of the two tori interchanged, except that the surface rotations are in the opposite direction. Because of the time reversibility of Stokes flow, reversing the direction of spin would change both the translational and rotational velocities by a minus sign. This sequence of rotation and reversing surface spin returns us to the original system, and we can conclude that $\Omega_1 = -\Omega_2$ and $\mathbf{U}_1 = \mathbf{U}_2$. Therefore, instantaneously, the tori have the same translational velocity but rotate in opposite directions. However, this need not be maintained as their dynamics evolves. We will see that depending upon their initial relative placements, the corotating pair can exhibit a rich array of dynamics.

Figure 11 shows a sequence of snapshots of corotating tori of unit diameter, aspect ratio $s_0 = 5$, rotational speed $u_0 = 100$, initially placed with a vertical offset between their centers of $h_1 = 1$, and a horizontal offset in the x direction of $h_2 = 0.5$. Although their translational velocities are equal, their rotational velocities are opposite. The individuals in this pair eventually move away from each other. Figure 12 shows a sequence of snapshots of the same corotating tori, but initially placed with a vertical offset between their centers of $h_1 = 0.2$, and a horizontal offset in the x direction of $h_2 = 1.6$. Because the pair is moving upwards, the frame of view is also moving upwards at a speed of 30. Examining the final frame [Fig. 12(h)], we see that this pair regains its original relative placement, and will continue on in a periodic orbit.

Tchieu *et al.* [26] studied the interaction of pairs of finite dipoles in two-dimensional inviscid flow. A finite dipole is a pair of equal and opposite strength vortices that are constrained to remain at a constant separation distance. The flow field

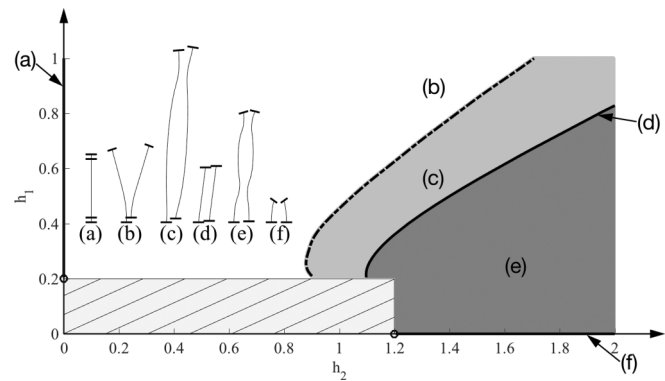


FIG. 13. Classification of all trajectories of centers of two corotating tori of unit diameter, aspect ratio $s_0 = 5$, and surface velocity $u_0 = 100$ for different vertical (h_1) offsets and horizontal offsets (h_2) in initial placement. In each case the normals of the tori were initially parallel, but not necessarily collinear. The inset at the left shows the trajectories of the centers of pairs of corotating toroidal swimmers for six initial offsets. (a) $h_1 = 1, h_2 = 0$ with final time $t = 0.2$. (b) $h_1 = 1, h_2 = 0.5$ with final time $t = 0.25$. (c) $h_1 = 0.4, h_2 = 1$ with final time $t = 0.6$. (d) $h_1 = 0.3, h_2 = 1.138$ with final time $t = 0.199$. (e) $h_1 = 0.2, h_2 = 1.6$ with final time $t = 0.4$, and (f) $h_1 = 0, h_2 = 1.6$ with final time $t = 0.083$. The regions in (h_1, h_2) phase space that correspond to the six qualitatively different trajectories (a)–(f) shown in the inset are labeled accordingly.

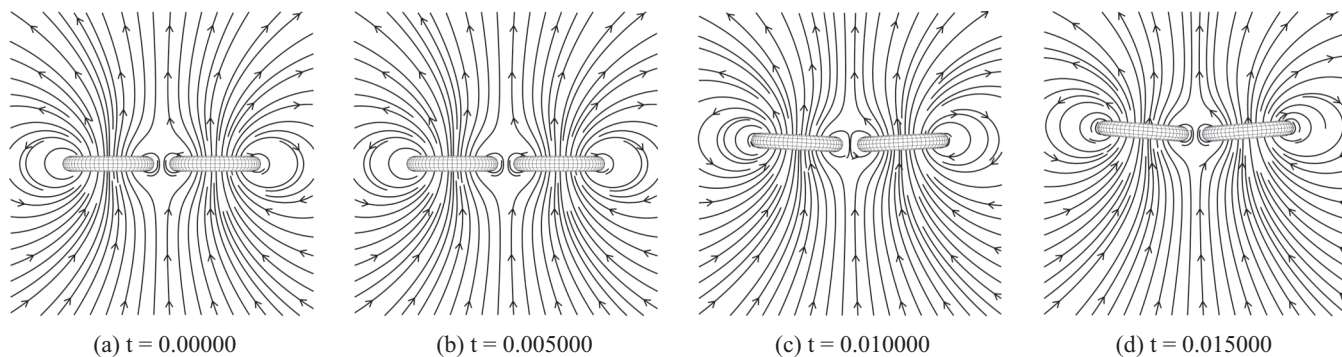


FIG. 14. Two tori with normals pointing upwards placed abreast.

generated by a single finite dipole in two dimensions around the dipole is much like the flow generated by a toroidal swimmer projected onto a plane of rotational symmetry about the toroidal normal. We find that trajectories of pairs of toroidal swimmers in three-dimensional Stokes flow are analogous to

the trajectories of finite dipoles in two-dimensional inviscid flow. The inset at the left of Fig. 13 shows the trajectories of the centers of pairs of corotating toroidal swimmers for six initial offsets. In all cases, the normals of the tori were parallel, but not necessarily collinear. Trajectory (a) shows

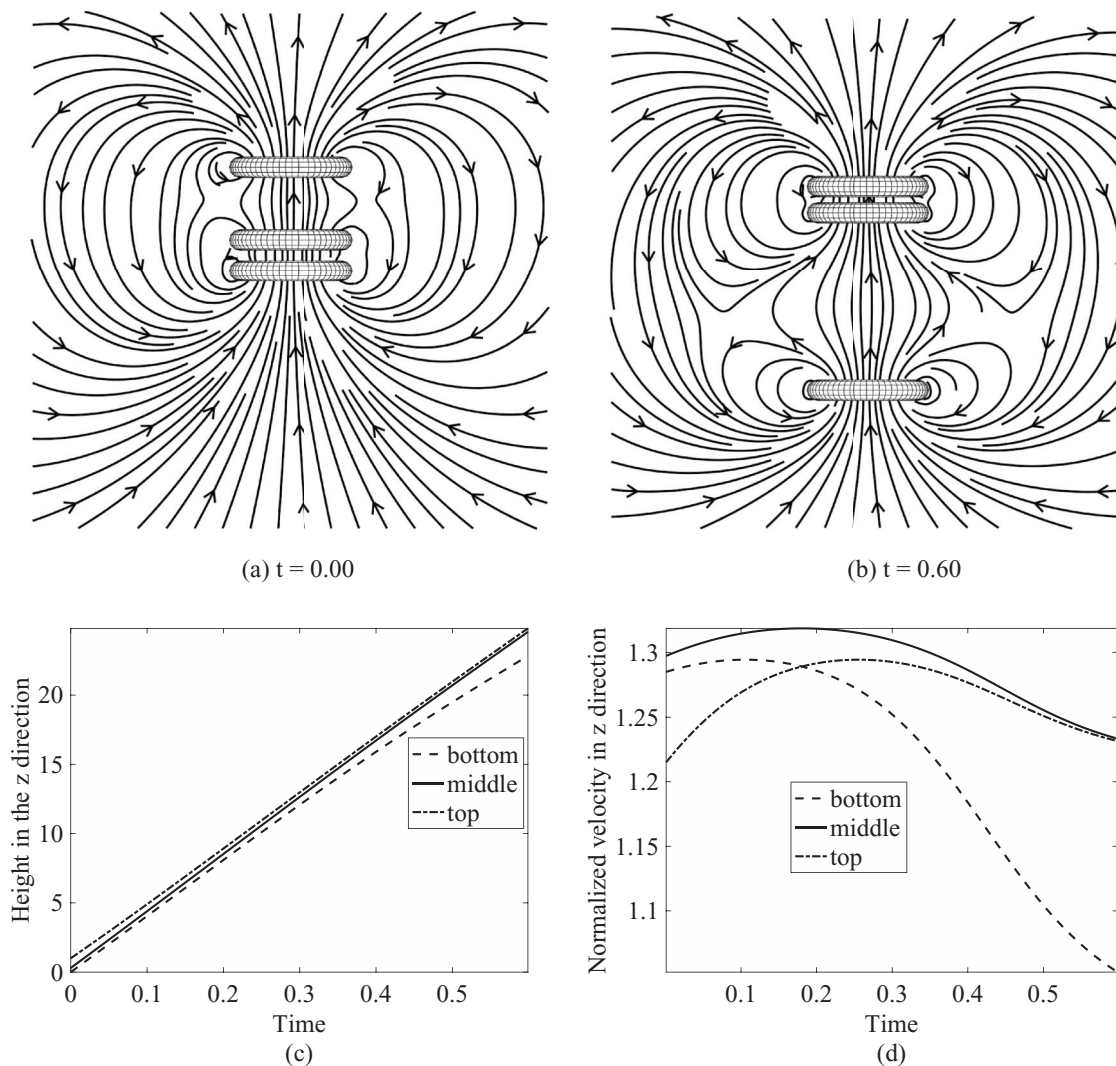


FIG. 15. (a) Three corotating tori placed in tandem with all normals pointing upward. (b) Positions of the three tori at time 0.60 with frame of view lowered by 24 units in z direction. (c) The trajectories of the z coordinates of the centers of the three tori. (d) The translational velocities of the three tori, normalized by that of an identical, isolated torus.

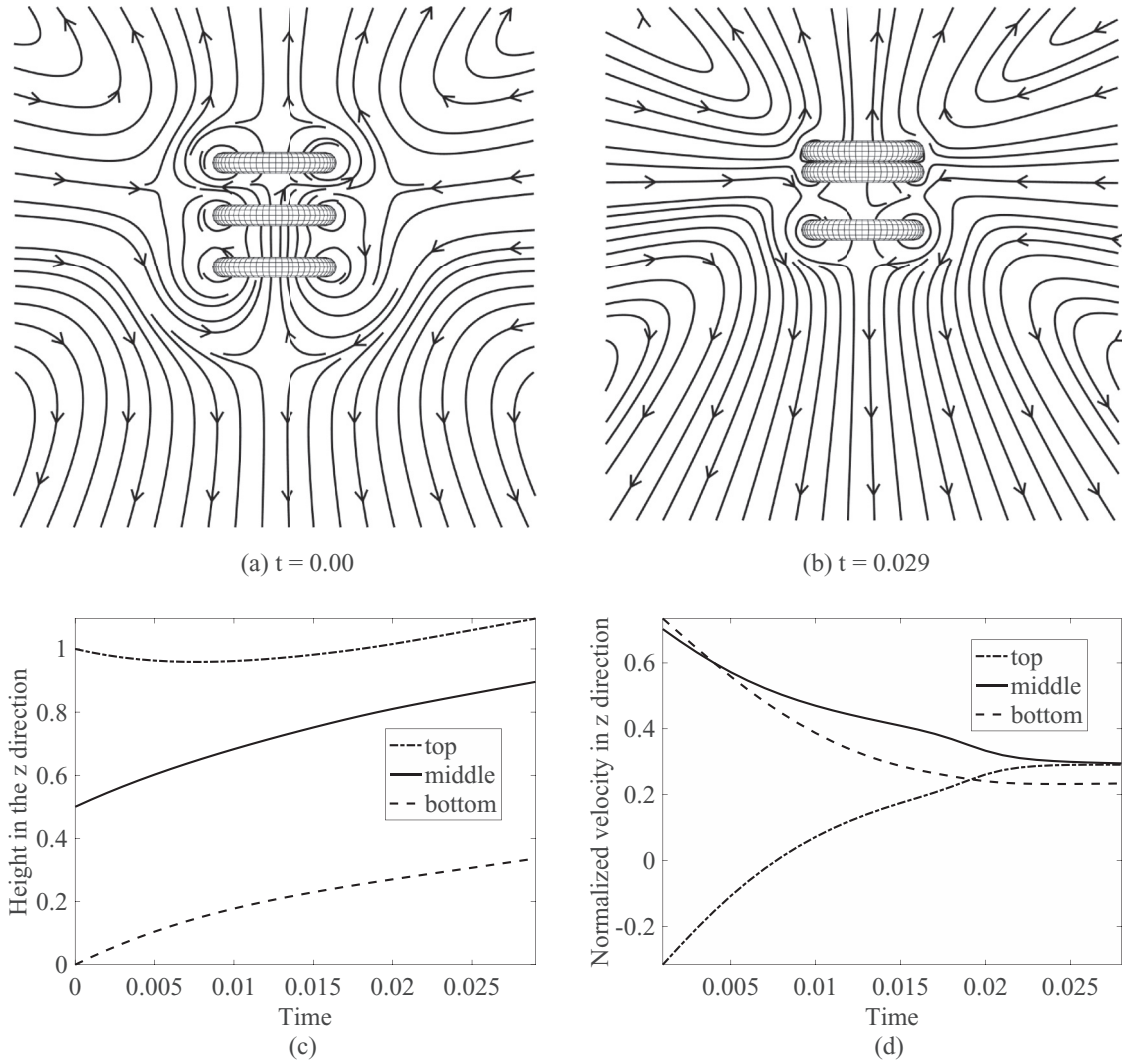


FIG. 16. Three tori placed in tandem. The surfaces of the bottom and middle tori rotate in the same direction, with normals pointing upwards. The top torus rotates counter to the others, with normal pointing downwards. (a) $t = 0.000$, (b) $t = 0.029$. (c) The trajectories of the z coordinates of the centers of the three tori. (d) The translational velocities of the three tori, normalized by the speed of an identical, isolated torus.

the perfectly in-tandem case from Fig. 4, where the tori swim upwards with the same velocity and do not rotate. Trajectory (b) shows an initial placement of tori whose paths eventually diverge. Trajectories (c) and (e) depict periodic trajectories, as in Fig. 12 discussed above. (Note that we have included movies of sample periodic orbits in the Supplemental Material [27].) Trajectory (d), like trajectory (a), is an equilibrium state where two tori translate with the same velocity and do not rotate. Finally, trajectory (f) shows a pair of corotating tori that were initially placed abreast. Using symmetry arguments, we note that two tori originally placed abreast and symmetric about the $y = 0$ plane as in Fig. 14(a) will rotate in opposite directions ($\Omega_1 = -\Omega_2$) and their translational velocities will satisfy $\mathbf{U}_1 = (u_1, 0, v_1)$ and $\mathbf{U}_2 = (-u_1, 0, v_1)$. The tori move upwards, but also turn in to face each other and the distance between their centers decreases.

In order to shed light upon the rich dynamics exhibited by the corotating pairs, we performed simulations where the

initial horizontal displacement h_2 and the vertical displacement h_1 between their centers were systematically varied. Figure 13 presents a phase diagram in (h_2, h_1) space that indicate when the different trajectories occur. First, we note that because of the nonzero toroidal radii, there is a hatched rectangular region, which must be excluded. The state (a) on the y axis ($h_2 = 0$) represents the perfectly in-tandem tori that move upwards as a pair. The state (f) on the x axis ($h_1 = 0$) depicts tori that move towards each other with mirror symmetry, and eventually collide. The states (c) and (e) represent periodic trajectories where the tori initially move away from each other (c) or move initially towards each other (e). These periodic states are separated in phase space by the curve (d), where the two exhibit no rotations. The offsets in region (b) lead to trajectories where the toroidal pair move away from each other—at least for the duration of the simulations. We see from this phase diagram that the in-tandem configuration is unstable: a slight horizontal offset will cause the pair to diverge.

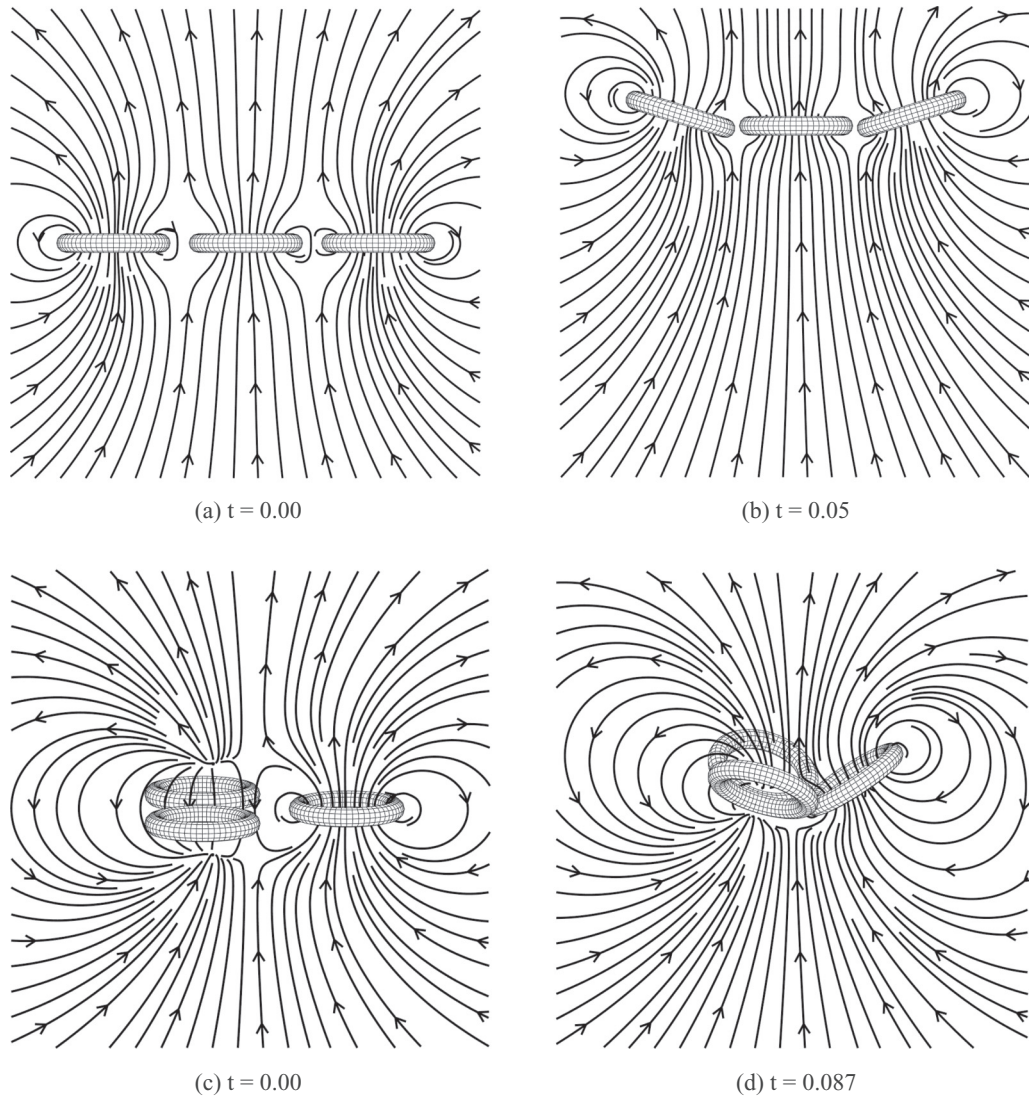


FIG. 17. (a) Three identical tori are placed with their centers collinear in the x - y plane. At $t = 0$ their normals point upwards. (b) The trio at $t = 0.05$. (c) Three identical tori are placed with their centers at vertices of an equilateral triangle in the x - y plane. At $t = 0$ their normals are pointing upwards. (d) The trio at $t = 0.087$, with frame of view decreased in z direction by two units.

C. Interaction of three tori

In the previous section we noted that when two identical corotating tori are placed in tandem, they experience no rotational velocity, but translate at the same velocity, keeping the distance between their centers fixed. This steady motion does not occur when three identical corotating tori are placed in tandem, even if they are initially equally spaced vertically. Symmetry arguments tell us that each will have zero rotational velocity, and the top and bottom tori will have the same translational velocity. However, the middle torus will experience a translational velocity bigger than the other two. Thus, equidistant spacing is lost. Figure 15(a) shows a snapshot of three identical corotating tori of unit diameter, aspect ratio $s_0 = 5$, $u_0 = 100$ (normals pointing upwards), initially placed so that the middle torus is closer to its bottom neighbor. Figure 15(b) shows the trio at a later time, where the frame of view in the z direction has been increased by 24 units. Figure 15(c) shows the progression of the z coordinate of the

centers of the three tori, and Fig. 15(d) shows their translational velocities normalized by that of an identical, isolated torus. We see that the velocity of the middle torus initially gets the largest boost from its neighbors, with the bottom torus lagging behind. Eventually, the top two move as a pair, and the bottom slows down nearly to the speed of an isolated torus.

Next we examine the interesting dynamics of three tori placed in tandem that are identical to the tori in Fig. 15 except for their directions of rotation [see Fig. 16(a)]. In this case, the surfaces of the bottom and middle tori are rotating in the same direction, with normals pointing upwards, but the surface of the top torus is rotating in the opposite direction (normal pointing downwards) at the same speed. The top torus, wanting to move downwards, has its progression inhibited by the top and middle torus, both wanting to move upwards. Figure 16(b) shows the relative configuration of the tori at a later time. Figure 16(c) shows the progression of the z coordinate of the centers of the tori and Fig. 16(d) shows their translational velocities normalized by the speed of an identical,

isolated torus. We see that while the top torus initially has a negative velocity, its velocity increases to the point where it moves upwards with the other two. Because each torus has a radius of $r_h = 0.1$, the distance between the centers of the middle and top tori can never be less than 0.2. In fact, we do terminate this simulation right before the collision of these tori occurs. We remark that this model enforces a prescribed surface velocity on each torus that does not change due to the state of the system. Because of this and the finite extent of the toroidal radii, interacting tori may collide in finite time. Future models could include feedback from the other tori that would adjust surface velocities, perhaps based upon a prescribed power input. In addition, repulsive forces could be included to eliminate collisions.

We conclude by visualizing the interaction of three tori placed abreast. Figure 17(a) shows an initial configuration where the centers of the tori are collinear. Symmetry arguments show that the middle torus will not rotate, but the outer two will rotate in opposite directions. Figure 17(b) shows the trio at a later time. Figure 17(c) shows an initial configuration of three tori whose centers are placed at vertices of an equilateral triangle. They each have the same rotational velocities and translational speeds. Figure 17(d) shows their configuration at a later time. Each torus rotates in the direction of the angle

bisector of the triangle, and they move towards each other like a flower folding its petals.

V. CONCLUSION

In this work we have considered the fluid dynamic interactions of classical toroidal swimmers that can propel themselves in a Stokesian fluid, not by shape changes, but by surface rotations. While these swimmers were proposed as hypothetical constructs [7,8] to provide insight into microorganism swimming, the propulsion of these tiny doughnuts is related to dinoflagellate motility [18] and has the potential to be used to design motile nanomachines [19]. Here we have used symmetry arguments and a regularized Stokeslet framework to examine the interactions of pairs and trios of free toroidal swimmers. In all of the simulations presented above, the rotational velocities of the surfaces of the toroidal swimmers were prescribed. This could lead to collision of nearby tori or very large power expenditures by a torus so that its imposed surface velocity is realized. It would be interesting to expand the model presented here by setting up a controlled system whereby the surface velocities of the tori are not prescribed, but evolve based upon the state of the system.

-
- [1] E. Lauga and T. Powers, *Rep. Prog. Phys.* **72**, 096601 (2009).
 - [2] H. Stone, A. Stroock, and A. Ajdari, *Annu. Rev. Fluid Mech.* **36**, 381 (2004).
 - [3] K. Son, D. Brumley, and R. Stocker, *Nature Rev. Microbiol.* **13**, 761 (2015).
 - [4] N. Koumakis, A. Lepore, C. Maggi, and R. Di Leonardo, *Nature Commun.* **4**, 2588 (2013).
 - [5] D. Weibel, P. Garstecki, D. Ryan, W. DiLuzio, M. Meyer, J. Seto, and G. Whitesides, *Proc. Natl. Acad. Sci. U.S.A.* **102**, 11963 (2005).
 - [6] S. Tottori, L. Zhang, K. Krawczyk, A. Franco-Obregon, and B. Nelson, *Adv. Mater.* **24**, 811 (2012).
 - [7] G. I. Taylor, *Proc. R. Soc. London A* **211**, 225 (1952).
 - [8] E. M. Purcell, *Am. J. Phys.* **45**, 3 (1977).
 - [9] A. T. Chwang and W.-S. Hwang, *Phys. Fluids A* **2**, 1309 (1990).
 - [10] R. M. Thaokar, H. Schiessel, and I. M. Kulic, *Eur. Phys. J. B* **60**, 325 (2007).
 - [11] A. M. Leshansky and O. Kenneth, *Phys. Fluids* **20**, 063104 (2008).
 - [12] F. J. Taylor, *Phycologia* **14**, 45 (1975).
 - [13] P. H. Leblond and F. J. Taylor, *BioSystems* **8**, 33 (1976).
 - [14] G. Gaines and F. J. Taylor, *J. Protozool* **32**, 290 (1985).
 - [15] M. Cachon, J. Cachon, J. Cosson, C. Greuet, and P. Huitorel, *Biol. Cell* **71**, 175 (1991).
 - [16] T. Fenchel, *Protist* **152**, 329 (2001).
 - [17] I. Miyasaka, K. Nanba, K. Furuya, Y. Nimura, and A. Azuma, *J. Exp. Biol.* **207**, 3055 (2004).
 - [18] H. Nguyen, R. Ortiz, R. Cortez, and L. Fauci, *J. Fluid Mech.* **671**, 574 (2011).
 - [19] I. Kulic, R. Thaokar, and H. Schiessel, *Europhys. Lett.* **72**, 527 (2005).
 - [20] T. Ishikawa, M. Simmonds, and T. Pedley, *J. Fluid Mech.* **568**, 119 (2006).
 - [21] T. Ishikawa and M. Hota, *J. Experiment. Bio.* **209**, 4452 (2006).
 - [22] Y. Yang, J. Elgeti, and G. Gompper, *Phys. Rev. E* **78**, 061903 (2008).
 - [23] S. D. Olson and L. J. Fauci, *Phys. Fluids* **27**, 121901 (2015).
 - [24] J. Huang, Ph.D. thesis, Tulane University, 2014 (unpublished).
 - [25] R. Cortez, L. Fauci, and A. Medovikov, *Phys. Fluids* **17**, 031504 (2005).
 - [26] A. A. Tchieu, E. Kanso, and P. K. Newton, *Proc. R. Soc. London A* **468**, 3006 (2012).
 - [27] See Supplemental Material at <http://link.aps.org/supplemental/10.1103/PhysRevE.95.043102> for movies of sample periodic orbits.
 - [28] C. Pozrikidis, *Boundary Integral and Singularity Methods for Linearized Viscous Flow* (Cambridge University Press, Cambridge, 1992).
 - [29] A. Aboelkassem, *Micromachines* **6**, 1143 (2015).
 - [30] V. Aranda, R. Cortez, and L. Fauci, *J. Biomech.* **48**, 1631 (2015).
 - [31] R. M. Thaokar, *Eur. Phys. J. B* **61**, 47 (2008).
 - [32] M. Wykes, J. Palacci, T. Adachi, L. Ristroph, X. Zhong, M. Ward, J. Zhang, and M. Shelley, *Soft Matter* **12**, 4584 (2016).